Journal of Colloid and Interface Science 672 (2024) 814–823

Contents lists available at ScienceDirect

Journal of Colloid And Interface Science

journal homepage: www.elsevier.com/locate/jcis

Regular Article

Effect of particle stiffness and surface properties on the non-linear viscoelasticity of dense microgel suspensions

Jacopo Vialetto [a,b,c,*], Shivaprakash N. Ramakrishna [b], Lucio Isa [b], Marco Laurati [a,c,*]

[a] Department of Chemistry "Ugo Schiff", University of Florence, via della Lastruccia 3, 50019 Sesto Fiorentino (FI), Italy
[b] Laboratory for Soft Materials and Interfaces, Department of Materials, ETH Zürich, Vladimir-Prelog-Weg 5, 8093 Zürich, Switzerland
[c] Consorzio interuniversitario per lo sviluppo dei Sistemi a Grande Interfase (CSGI), via della Lastruccia 3, 50019 Sesto Fiorentino (FI), Italy

GRAPHICAL ABSTRACT

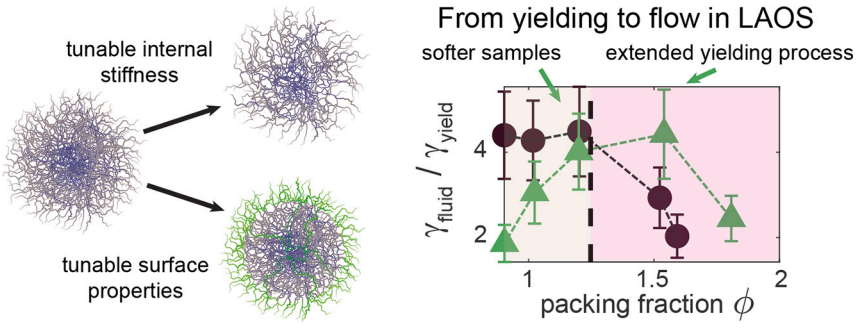

ARTICLE INFO

Keywords:
Colloidal particles
Large-amplitude oscillatory shear (LAOS)
Yielding
Rheology
Microgels
Atomic force microscopy

ABSTRACT

Hypothesis: Particle surface chemistry and internal softness are two fundamental parameters in governing the mechanical properties of dense colloidal suspensions, dictating structure and flow, therefore of interest from materials fabrication to processing.

Experiments: Here, we modulate softness by tuning the crosslinker content of poly(N-isopropylacrylamide) microgels, and we adjust their surface properties by co-polymerization with polyethylene glycol chains, controlling adhesion, friction and fuzziness. We investigate the distinct effects of these parameters on the entire mechanical response from restructuring to complete fluidization of jammed samples at varying packing fractions under large-amplitude oscillatory shear experiments, and we complement rheological data with colloidal-probe atomic force microscopy to unravel variations in the particles' surface properties.

Findings: Our results indicate that surface properties play a fundamental role at smaller packings; decreasing adhesion and friction at contact causes the samples to yield and fluidify in a lower deformation range. Instead, increasing softness or fuzziness has a similar effect at ultra-high densities, making suspensions able to better adapt to the applied shear and reach complete fluidization over a larger deformation range. These findings shed new light on the single-particle parameters governing the mechanical response of dense suspensions subjected to deformation, offering synthetic approaches to design materials with tailored mechanical properties.

* Corresponding authors.
E-mail addresses: jacopo.vialetto@unifi.it (J. Vialetto), marco.laurati@unifi.it (M. Laurati).

https://doi.org/10.1016/j.jcis.2024.05.214
Received 7 May 2024; Received in revised form 24 May 2024; Accepted 28 May 2024
Available online 3 June 2024

1. Introduction

Dense suspensions of colloidal particles are at the core of a variety of materials and processes, being fundamental components in formulations for surface coatings, fluids for oil extraction, additive manufacturing, cosmetics, food-grade materials, etc. [1,2]. In addition to the particle surface properties, which dictate the strength of the main interparticle interactions at play (e.g., electrostatic, steric, van der Waals) the internal degree of softness of the colloids dramatically affects their behavior in crowded states, and it is used as a precisely controllable parameter to tune their structural and rheological properties [3,4]. This is of great interest for the fundamental understanding of the rich phase behavior of a broad range of soft systems, including biological ones [5,6], and for the design of functional materials with tuneable mechanical responses, as required in applications ranging from optics to viscosity modifiers and biocompatible carriers [7–13].

Among soft colloids, microgel particles made of swellable polymer networks offer multiple opportunities to achieve the desired functionalities in dense systems. When dispersed in a good solvent they are highly deformable, compressible, and can interpenetrate with neighboring particles [14,15], allowing one to easily reach states with effective volume fractions that exceed the hard-sphere limit, and can be higher than 1 [3,16,17]. The extent of deformation can be tuned at the synthesis level by varying the crosslinker content, or by using polymers responsive to external inputs (e.g., temperature, pH, ionic strength) [4]. This has a profound effect on the phase diagrams, flow and rheological properties of microgels in densely packed states, both in suspensions [15,18–23] and in two-dimensions (i.e., when microgels are compressed on a fluid interface) [24–26]. Tuning their internal elasticity allows, for example, to shift the transition between liquid and crystalline state to higher effective concentrations [22,24], to crystallize suspensions even in the presence of very high polydispersity [27,28], or to modulate the material viscoelastic properties such as storage modulus and yield strain [29,30].

The rheological response of microgel suspensions can be further modified acting on the interparticle contacts, consequently tuning the resulting interactions. For example, temperature variations in the case of poly(N-isopropylacrylamide) (pNIPAM) microgels allow inducing transitions from a more hydrophilic to a more hydrophobic surface, modifying the polymer conformation on the particle periphery and triggering the emergence of attractive interactions [31,32]. Alternatively, different polymers on the surface can be exploited to modulate the extent of adhesion, friction and interdigitation between particles [33–38]. Polyethylene glycols (PEG) are intriguing candidates in this regard, especially when considering potential applications requiring biocompatibility and enhanced particle stability for healthcare applications. PEG polymer chains are extensively used to modulate the self-assembly of block copolymers, such as pNIPAM-co-PEG chains that form micelles and aggregates by non-covalent interactions and find numerous applications as thermoreversible gelators [10,11,39,40], or to design microgel particles via covalent modification of the polymer network for an improved control over their structure and stimulus responsivity [36,41,42]. However, surface effects, albeit of utmost importance to fully comprehend the behavior of soft-particle systems, are rarely linked [32,34,43,44] to the complex rheological properties of dense microgel suspensions, and the separate contribution of particle's surface and bulk properties to the yielding process have not been fully considered.

In this work we focus on the linear and non-linear rheological behavior of dense pNIPAM microgel suspensions in the jammed state under oscillatory shear [45], with specific emphasis on the role of the internal degree of softness and the influence of particle surface properties. Although their viscoelastic response, particularly the yielding transition, have been already investigated previously [16,18,20,30,46,47], the full dynamics of yielding and the path towards complete fluidization under large amplitude oscillatory shear (LAOS) are still largely unexplored. Indeed, conventional analyses based on viscoelastic moduli calculated in first harmonic approximation typically determine a single yield strain or stress value, while the transition to flow is a progressive process that spans a broad range of applied deformations or stresses, from the values associated to initial restructuring to those corresponding to complete fluidization. Furthermore, studies that considered anharmonic contributions through Fourier Transform rheology did not take into account the whole spectrum of higher harmonics. Finally, only the analysis of the variation of the viscoelastic moduli along each deformation cycle can precisely reveal the onset of significant restructuring and yielding, as well as the complete reorganization of the local structure inducing flow [48,49].

Here, we analyze the effect of crosslinking density and that of adding linear PEG chains on the particle surface to tune their mechanical, adhesion and frictional responses by affecting preferentially the internal particle elasticity or the interactions at contact. We take advantage of the sequence of physical processes (SPP) [48,49] approach to analyze LAOS measurements in order to consider the whole spectrum of anharmonic contributions. This allows us to gain insights on the viscoelastic non-linear response during progressive fluidization of the samples at increasing applied deformations. By looking at LAOS data we, in particular, disclose the influence that particle softness and surface properties have in governing their rheological behavior in very high density states. In particular, we reveal that these parameters affect in a complex way the entire transition from the onset of yielding to the complete fluidization of the system, an information that could only be collected with the used approach. Additionally, to corroborate the rheological data, we employ colloidal probe atomic force microscopy (CP-AFM) to characterize the variation in the particles' adhesive and frictional properties mediated by the incorporation of PEG comonomers on the microgel surface.

2. Materials and methods

2.1. Reagents

N,N'-methylenebis(acrylamide) (BIS, Fluka 99.0%), potassium persulfate (KPS, Sigma–Aldrich 99.0%) and polyethylene glycol methyl ether methacrylate (PEGMA) m.w.: 13000 (abcr GmbH) were used without further purification. N-isopropylacrylamide (NIPAM, TCI 98.0%) was purified by recrystallization in 40/60 v/v toluene/hexane.

2.2. Microgels synthesis

pNIPAM microgels. pNIPAM microgels were synthesized by surfactant-free semi-batch radical precipitation polymerization, following already published protocols [50]. NIPAM (2g) and BIS were dissolved in 100 mL of MilliQ water. The amount of BIS was chosen in order to synthesize microgels with 5 or 1 mol % crosslinker. The monomers mixture was purged with nitrogen for 1 h and then 60 mL of the monomer solution was taken out with a syringe. 20 mL of MilliQ water were added to the reaction flask and the solution was immersed into an oil bath at 80 °C and purged with nitrogen for another 30 min. The reaction was started by adding 25 mg of KPS previously dissolved in 2 mL of MilliQ water and purged with nitrogen. Feeding of the monomer solution to the reaction flask was set at 0.5 mL/min and was initiated after 1.5 min. The reaction was quenched at the end of the feeding step by opening the flask to let the air in, and placing it in an ice bath. The colloidal suspension was dialysed for a week, and purified by 6 centrifugation cycles and resuspension of the sedimented particles in pure water, and freeze-dried.

pNIPAM-PEG microgels. pNIPAM-PEG microgels were synthesized by surfactant-free semi-batch radical precipitation polymerization, modifying already published protocols [36,42]. NIPAM (1g) and BIS were dissolved in 100 mL of MilliQ water. The amount of BIS was chosen in order to synthesize microgels with 5 or 1 mol % crosslinker, calculated with respect to all the monomers in the reaction mixture. Separately,

Table 1
Microgels used in this study, particle size at 19 °C, swelling ratio and k.

Microgel	mol % BIS	mol % PEGMA	d_h (19 °C) [nm]	d_h (19 °C) / d_h (45 °C)	k
pN5	5	-	826 ± 10	1.77 ± 0.04	7.55 ± 0.2
pN1	1	-	850 ± 8	2.16 ± 0.04	14.2 ± 0.2
pN-PEG5	5	1	847 ± 20	1.78 ± 0.05	8.0 ± 0.1
pN-PEG1	1	1	1013 ± 11	2.24 ± 0.05	21.6 ± 0.7

PEGMA (1.2g) dissolved in 20 mL of MilliQ water and KPS (16 mg) dissolved in 2 mL of MilliQ water were purged with nitrogen for 1 h. The reaction was carried out at 70 °C and it was started by adding KPS to the reaction flask containing NIPAM. After 20 min, the PEGMA monomer was injected in the flask at 0.33 mL/min. The reaction was stopped after 5 h 20 min by opening the flask and placing it in an ice bath. The colloidal suspension was dialysed for a week, purified by 6 centrifugation cycles and resuspension of the sedimented particles in pure water, and freeze-dried.

2.3. Experimental methods

DLS. Dynamic light scattering (DLS) experiments were performed using a Zetasizer (Malvern, UK). The microgels were redispersed in Milli-Q water at a concentration of 0.01 wt% in order to analyze samples in the dilute regime. The temperature was varied from 19 to 51 °C with 2 °C steps and 15 min equilibration time. For each temperature we recorded four consecutive measurements of 15 runs each.

Viscometry. Viscosity measurements were performed using a Micro-Ubbelohde viscometer (type no. 538 13, Xylem Analytics, Germany, capillary diameter 0.53 mm, constant K = 0.03) immersed in a water bath with a thermostat set at 25 °C. We measured the relative viscosity of diluted microgel suspensions at different concentrations with respect to that of pure water. For each concentration, the Micro-Ubbelohde viscometer filled with the microgel suspension was immersed at 25 °C for 10 minutes to ensure temperature equilibration prior to start the measurement. Successively, flow times were measured 5 times. The viscosity data were then fitted with the Einstein–Batchelor relation $\eta_{rel} = 1 + 2.5\phi + 5.9\phi^2$ with $\phi = k \cdot wt\%$, to determine the constant k and estimate the particle effective volume fraction ϕ. We note that the effective volume fraction in dense samples is only estimated with this equation as a quantitative knowledge of the variation of the microgel size with concentration is currently unknown for our systems.

Colloidal probe AFM (CP-AFM). Microgel monolayers were deposited onto silicon wafers via transferring from a hexane-water interface following procedures already described elsewhere [25,26]. Briefly, microgels were first adsorbed at the hexane-water interface, where they formed ordered monolayers. A piece of a silicon wafer, previously cleaned with a UV-ozone cleaner (UV/Ozone Procleaner Plus, Bioforce Nanosciences) for 15 minutes to ensure a highly hydrophilic surface, was then lifted from the water subphase (where it was immersed prior to forming the microgel monolayer) through the interface at a constant speed of 25 $\mu m \cdot s^{-1}$. This ensured transferring of the monolayer from the fluid interface to the solid substrate. The silicon wafer was then lifted out of the hexane phase, left to dry and successively re-immersed in Milli-Q water for performing the AFM measurements. We confirmed the sufficient stability of the microgel monolayer adsorbed on the solid substrate by imaging the substrate immersed in Milli-Q water twice on the same position using a sharp tip. As reported in Fig. S14, no discernible removal of particles was observed during the scanning process within the same applied load range we used for the friction experiments. Importantly, it should also be noted that the use of a colloidal probe for friction and force experiments decreases the contact pressure exerted by the probe to the microgels with respect to a sharp tip. Moreover, during the friction test approximately 7 friction loops were recorded across the sample surface on the same position. The consistency of these loops from the initial to the final one indicates the absence of significant particle removal during measurement.

Colloidal probe lateral force and adhesion force measurements were carried out using a MFP3D atomic force microscope (Asylum Research, Oxford Instruments, Santa Barbara, USA). The colloidal probe was prepared by gluing a silica colloid (16 μm in diameter, EKA Chemicals AB, Kromasil R, Sweden) to a tipless cantilever (CSC38, MikroMasch, Bulgaria) using a custom made micromanipulator. The prepared colloidal probe was treated under UV-ozone cleaner (Ossila, UK) for 20 minutes before the measurements. Friction loops were recorded by scanning the cantilever laterally over the microgel monolayer deposited on silicon surface, immersed in Milli-Q water at 25 °C, with a scan rate of 0.5 Hz and an applied load of ~10 nN. The temperature was kept constant by using a bio heater cell (MFP 3D, Asylum research, Oxford instrument). The normal and torsional spring constant calibration of the cantilever was performed by using thermal noise [51] and Sader's method [52], respectively. The lateral-force calibration was carried out by employing the 'test-probe method' [53].

Adhesion measurements were performed using the same cantilever and on the same samples right after the friction tests. Force versus distance curves were measured at a scanning speed of 1 $\mu m/s$.

Rheology. Rheological measurements were performed using a Discovery HR-3 rheometer (TA Instruments), with a plate-plate geometry (stainless steel, diameter: 40 mm). The choice of this geometry is due to the relatively high viscosity of the samples, which would require application of a significantly high normal stress to the sample during loading in a cone-plate geometry, possibly altering its structural arrangement before application of shear. The non-uniform stress distribution in the sample associated with the plate-plate geometry results in quantitative differences in the LAOS parameters describing anharmonic contributions compared to cone-plate measurements [54–56]. However, trends of the same parameters discussed in this work are not significantly affected [56]. We also note that, when using this configuration, no indications of responses associated with wall-slip are observed.

A Peltier in contact with the lower plate ensured a constant temperature of 25 °C, and a solvent trap consisting of an enclosure with a solvent seal at the top and a wet tissue adhered to its interior was used to avoid evaporation. The gap in all experiments was set to 250 μm. A rejuvenation protocol was implemented before each measurement to minimize variabilities due to sample loading and aging. We first applied an oscillatory shear for 120 s with a large strain amplitude (γ = 600%) at frequency ω = 1 rad/s, during which all samples showed a liquid-like behavior. We then applied a second oscillatory shear with a low strain amplitude (γ = 0.5%) at frequency ω = 10 rad/s, until a steady state response in the viscoelastic moduli was reached. For all samples, such a steady state response was obtained within 120 s. Frequency sweep experiments were performed at γ = 0.1%, varying ω from 100 to 0.1 rad/s. Oscillatory shear experiments as amplitude sweeps were performed at constant frequency, with strain γ varying from 0.5% to 1000%. For each point, we recorded 5 cycles; for each sample, we tested two frequencies, ω = 10 and 1 rad/s.

All time-resolved raw data were processed by using a freely available MATLAB-based software developed by Rogers [49]. The data analysis is based on the sequence of physical processes (SPP) technique, which is used to define the instantaneous moduli (G_t' and G_t'') throughout the time-varying response of the material to deformation, for each applied oscillatory shear. A complete derivation of the SPP parameters can be found elsewhere [48,49]. The SPP analysis was performed on data reconstructed via Fourier-domain filtering, using 5 harmonics. In short,

Table 2
Definitions of the metrics used to investigate the rheological response under LAOS.

metric	definition
γ_h	$max(G_t') > 1.05 \cdot G'$
γ_{yield}	$max(\delta_t) = \pi/4$
γ_{fluid}	$max(\delta_t) = \pi/2$

for each oscillatory shear at fixed strain the analysis capture the instantaneous moduli G_t' and G_t'', which describe the instantaneous response of the material within the cycle. The non-linear response of the material to deformation can be expressed in terms of the instantaneous magnitude of the viscoelastic response:

$$|G_t^*| = \sqrt{G_t'^2 + G_t''^2} \tag{1}$$

and the phase angle of the complex modulus:

$$\delta_t = \tan^{-1}\left(\frac{G_t''}{G_t'}\right) \tag{2}$$

As in the linear viscoelastic regime, yielding of a material can be identified on a macroscopic scale as the point within the cycle when the instantaneous response changes from primarily elastic, $\delta_t < \pi/4$, to primarily viscous, $\delta_t > \pi/4$. This corresponds to a crossover between the time-resolved instantaneous moduli G_t' and G_t'', analogous to the crossover between G' and G'' in the first harmonic approximation. As described in the works of Rogers [49], the range in which $\pi/4 < \delta_t < \pi/2$ can be considered as incomplete yielding of the material, when a significant degree of internal structure is maintained. Instead, complete yielding (i.e., completely unstructured state) can be defined as when the phase angle goes to the viscous limit of $\delta_t = \pi/2$. In this work we introduce another metric (γ_h) defined as $max(G_t') > 1.05 \cdot G'$, to estimate when the rheological response within the deformation cycle starts to differ from the response in the first harmonic approximation. A summary of the definitions of these three metrics is reported in Table 2. The error on the characteristic yield strain values was estimated from the limitation in the resolution of the strain determination imposed by the finite sampling used for each LAOS experiment.

3. Results and discussion

In Fig. 1a we report a schematic of the microgels synthesized and analyzed in this work. We investigated pNIPAM microgels with 5 and 1 mol% crosslinker (identified as pN5 and pN1, respectively), as well as pNIPAM-PEG microgels with 5 and 1 mol% crosslinker (pN-PEG5 and pN-PEG1, respectively) and 1 mol% of polyethylene glycol methyl ether methacrylate (PEGMA, m.w.: 13000). Details on the synthesis protocols are in the Materials and Methods section. Importantly, the use of a semi-batch protocol, together with the lower reaction constant of long PEGMA chains with respect to NIPAM, is believed to effectively accumulate the linear PEG comonomers on the microgels' surface [42,57].

Dynamic light scattering is used to quantify the hydrodynamic diameter (d_h) of the different microgels as a function of temperature (Fig. 1b and S1). Both the sharpness of the transition and the swelling ratio (see also Table 1) are not affected by the addition of PEG, and the swelling ratio only depends on the crosslinker content. This is in accordance with a particle architecture composed of PEG chains located mainly on the particle periphery that do not influence the thermal response of the pNIPAM network [57,58]. The fact that the deswelling is nearly the same for particles with the same crosslinker content (Fig. 1b) supports the assumption that PEG chains do not modify the effective crosslinking density and therefore the single-particle internal elasticity.

3.1. Non-linear rheology of pNIPAM microgels

We begin by analyzing the rheological response of pN5 microgels at varying effective volume fractions (ϕ) beyond close packing, i.e. starting at 0.9. The linear viscoelastic moduli obtained from frequency sweeps (Fig. S2a) indicate a solid-like response for all samples, with the storage modulus G' always higher than the loss modulus G''. The plateau viscoelastic moduli increase linearly with ϕ (Fig. S2b), as expected for pure pNIPAM microgels at comparable concentrations [16,36,59], and as ascribed to the finite softness of their cores [20,33,60]. This result is indicative of affine elasticity, as reported by theory and simulations at comparable oscillation frequencies [61]. We note that all samples are well within the jamming limit as estimated by Pellet and Cloitre [20]. The microgels are therefore expected to be highly deformed, compressed and possibly interpenetrated [15].

We then investigate the non-linear response in LAOS experiments. In Fig. 2a we report G' and G'' measured in first harmonic approximation, for an oscillation frequency $\omega = 10$ rad/s. For all samples, the moduli are approximately constant up to strain amplitudes (γ) of a few percent, while at larger applied strains the material response changes from predominantly solid-like ($G' > G''$) to liquid-like ($G' < G''$), exhibiting a weak G'' overshoot behavior that has been recently associated to a continuous transition from recoverable to unrecoverable deformation [62]. This response is in line with results typically reported for microgels [16,18,20,30], hard-core soft-shell particles [46,63], and other colloidal systems with varying softness [3].

We used the time-resolved SPP analysis [48,49] (see Materials and Methods) to get detailed insights into the non-linear behavior of the samples as a function of the applied strain and to obtain information on the dynamics of the mechanical response during the yielding transition. Fig. 2b shows Cole-Cole plots of the variation of the instantaneous moduli G_t' and G_t'' during the cycles for increasing γ (color-coded from blue to yellow) for pN5 microgels at $\phi = 1.59$. At low applied strains $G_t' >> G_t''$ for the entire cycle, as expected for a solid-like response. Upon increasing γ, G_t' decreases, G_t'' increases, and both moduli change significantly during the oscillation cycle. For this sample, we observe that G_t'' becomes higher than G_t', corresponding to a partial yielding of the material within the cycle [49], starting from $\gamma = 22.7\%$ (arrow in Fig. 2b). The instantaneous moduli are then used to calculate the instantaneous phase angle δ_t (eq. (2)) as defined by Donley et al. [49], which is used to identify the point within the cycle when the material response changes from primarily elastic, $\delta_t < \pi/4$, to primarily viscous, $\delta_t > \pi/4$, up to a completely unstructured state $\delta_t > \pi/2$ (see Materials and Methods). Fig. 2c reports the variation of δ_t within the cycle at $\gamma = 22.7\%$, clearly showing the phase angle crossing the $\pi/4$ line, corresponding to partial yielding at this γ. A further increase in γ in successive cycles results in δ_t plots where both the time during the cycle in which $\delta_t > \pi/4$, and its maximum value, increase.

To explore in details the yielding transition under oscillatory shear, we extracted three metrics from the time-resolved SPP analysis in order to identify when the material's response departs from a primarily solid-like behavior, then yields and finally fluidifies at very large applied deformations. We first define γ_h as the strain for which $max(G_t') > 1.05\,G'$ (see Fig. 2e, where γ_h is visualized for $\phi = 1.59$, and Fig. S3 for similar plots for the other ϕ). This metric allows us to unambiguously identify from which strain value the time-resolved analysis differs from the response of the harmonic approximation, indicating an appreciable sample reorganization within each deformation cycle. The value of $max(\delta_t)$ (Fig. 2d), i.e. the maximum of the δ_t vs strain curves obtained for each applied strain (see an exemplary curve in Fig. 2c), is then used to summarize the time-resolved analysis and describe the yielding process. The first strain value at which $max(\delta_t) = \pi/4$ pinpoints when the material starts yielding (γ_{yield}); while we identify the strain at which the material fully fluidifies (γ_{fluid}) with the first strain value at which $max(\delta_t) = \pi/2$.

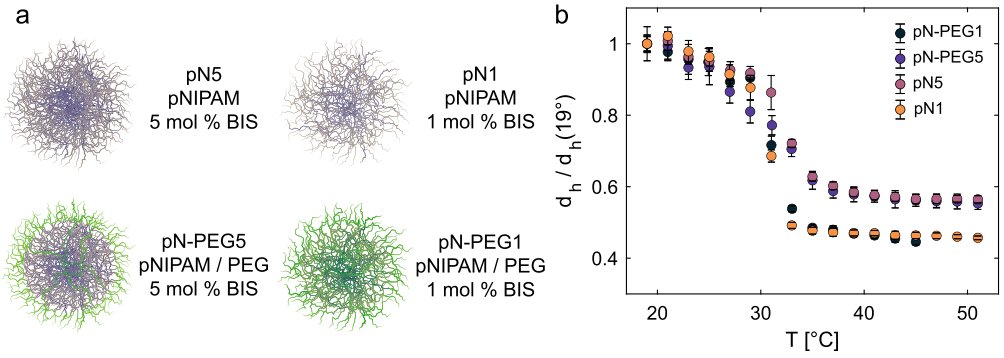

Fig. 1. pNIPAM and pNIPAM-PEG microgels. a) Sketch of the microgels synthesized and investigated in this work. b) Microgels' swelling ratio as a function of temperature measured as $d_h/d_h(19\,°C)$, where d_h is the hydrodynamic diameter.

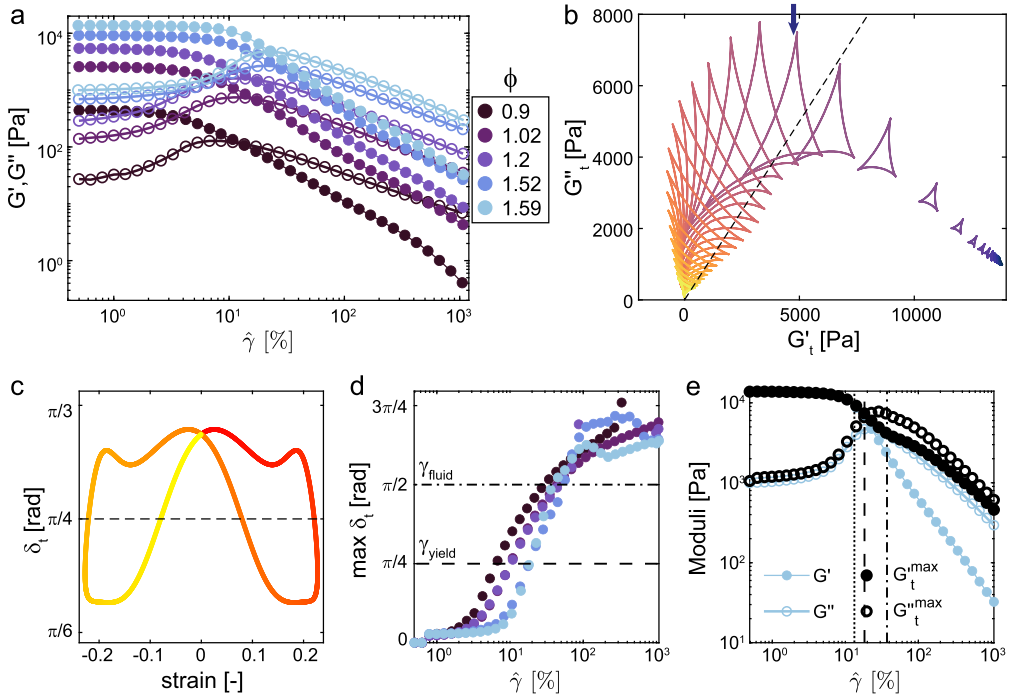

Fig. 2. LAOS of pN5 microgels. a) Storage (G', solid symbols) and loss (G'', open symbols) moduli from strain amplitude sweeps at 25 °C and $\omega = 10$ rad/s at increasing effective volume fraction (ϕ). b) Instantaneous values of the time-resolved viscoelastic SPP moduli G'_t and G''_t for pN5 microgels at $\phi = 1.59$. Color-coding from blue to yellow indicates increasing γ% in the amplitude sweep experiment. The dashed line marks the yielding threshold $\delta_t = \pi/4$. c) Plot of the instantaneous phase angle δ_t corresponding to the data at $\gamma = 22.7\%$ in (b) indicated by the arrow. Color-coding from red to yellow shows the time within one oscillation cycle. d) $max(\delta_t)$ as a function of strain amplitude in amplitude sweep experiments at increasing ϕ. The dashed and the dash-dotted lines indicate γ_{yield} and γ_{fluid}, respectively. e) Detail of the amplitude sweep for $\phi = 1.59$. The black solid and open symbols represent $max(G'_t)$ and $max(G''_t)$, respectively. The dotted line indicates γ_h, the dashed line γ_{yield} and the dash-dotted line γ_{fluid} (see main text). (For interpretation of the colors in the figure(s), the reader is referred to the web version of this article.)

We first discuss results obtained investigating pN5 microgels at increasing concentration: Fig. S4a reports γ_h values, while γ_{yield} and γ_{fluid} metrics are shown in Fig. 3 (black symbols). The strain values related to these metrics increase as a function of ϕ. This can be expected, as more concentrated samples become stiffer and can accommodate larger deformations before the internal structure breaks, and the sample yields and flows. A similar result is observed also when looking at the crossover point $G' = G''$ in the harmonic approximation (Fig. S4b), typically considered as an indication of the yielding transition in the sample [16,18,64–66]. The values of γ_{yield} (i.e., when $G'_t = G''_t$) are always lower than the corresponding $G' = G''$ (γ_{CR}, Fig. S4c): partial yielding within a deformation cycle happens before the actual crossover of the harmonic moduli, as already observed for similar samples [49]. Interestingly, the distance between these two metrics, γ_{yield} and γ_{CR}, decreases as a function of ϕ. We attribute the latter result to a more abrupt onset of the yielding transition upon increase in particle density.

We note that the apparent decrease of γ_{fluid} at $\phi = 1.59$ is attributed to noise in the acquired data. When the same analysis was applied for strain amplitude sweeps at $\omega = 1$ rad/s (Fig. S5), the obtained value of γ_{fluid} at $\phi = 1.59$ is comparable to that at $\phi = 1.52$ (Fig. S5e). Fig. S5 also shows that these results are independent of the oscillation frequency.

We then quantified the deformation span required for each transition to occur; in other words, the abruptness of yielding as a function of ϕ. This is measured by the strain ratios $\frac{\gamma_{yield}}{\gamma_h}$ (Fig. 3d) and $\frac{\gamma_{fluid}}{\gamma_{yield}}$ (Fig. 3e), indicating, respectively, how much deformation of the sample is required to cause an appreciable modification of the internal structure until partial yielding occurs, and how much deformation can the material sustain before it completely yields. Both ratios are approximately

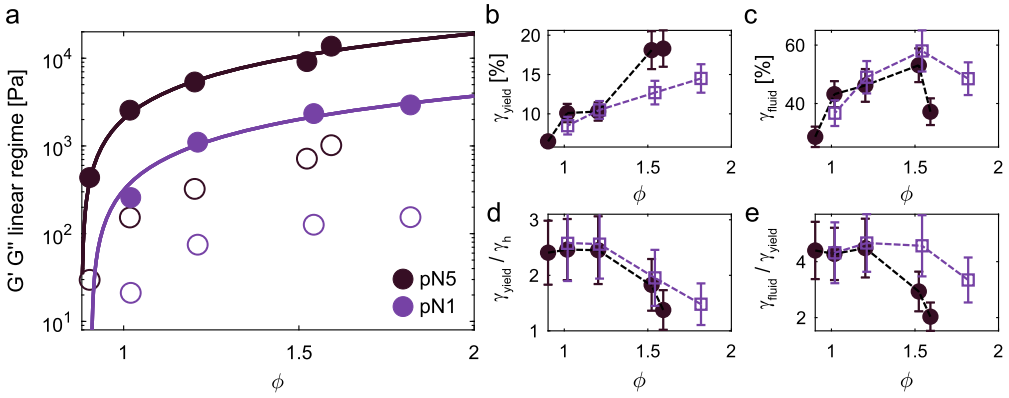

Fig. 3. Effect of crosslinking density. a) Storage (filled symbols) and viscous (open symbols) moduli in the linear regime ($\gamma = 0.5 - 1\%$) as a function of ϕ (temperature = 25 °C, $\omega = 10$ rad/s). Solid lines represent linear fitting of the data. b) First strain value at which $\delta_t = \pi/4$ as a function of volume fraction. c) First strain value at which $\delta_t = \pi/2$ as a function of volume fraction. d) Strain ratio $\frac{\gamma_{yield}}{\gamma_h}$ as a function of volume fraction. e) Strain ratio $\frac{\gamma_{fluid}}{\gamma_{yield}}$ as a function of volume fraction. In b-e) pN5 filled circles, pN1 open squares, dashed lines to guide the eye.

constant up to $\phi = 1.2$. In this volume fraction range, the transitions, even though all starting at higher absolute strain values, require a similar, relative, deformation range. This is visually captured also in Fig. S3, where the γ relative to each metric is superimposed on the G', G'' moduli from LAOS.

A different behavior is instead observed at higher ϕ, for which both ratios decrease. We attribute this effect to the extent of compression, deformation and interpenetration of the microgels in the structure as a function of ϕ. In the extreme cases, $\phi > 1.2$ for this particular microgel, the particles are already significantly deformed at rest and can adapt less to the imposed sample deformation. As a consequence, the yielding transition, even though starting at higher (absolute) deformation values due to the increased sample stiffness, is sharper, i.e. takes place within a smaller deformation range. We point out that this behavior resembles that of hard spheres, for which the yielding transition occurs more abruptly than for softer particles [46].

3.2. Effect of crosslinking density

We then performed the same analysis on pN1 microgels (Figs. S6-S7) to quantify the influence of the single-particle internal elasticity on the rheological behavior in suspension. As for the stiffer pN5 microgels, the storage modulus increases linearly with ϕ at low deformations (Fig. 3a). For comparable ϕ, we observe, as expected, a decrease in G', G'' values for microgels with lower crosslinker content, indicating softer samples at rest [29].

The non-linear response as a function of ϕ is however more complex. In the lower ϕ range, we do not detect any appreciable difference in the onset of the yielding transition (Fig. S8 and Fig. 3b) and fluidization (Fig. 3c) as a function of crosslinking density, despite the lower values of the corresponding linear moduli. Instead, for the more concentrated samples ($\phi > 1.5$) the increased softness of pN1 microgels shifts the onset of yielding to lower deformation values, but then complete fluidization requires larger strains (Fig. 3c). This result is clearly captured by the strain ratios $\frac{\gamma_{yield}}{\gamma_h}$ (Fig. 3d) and $\frac{\gamma_{fluid}}{\gamma_{yield}}$ (Fig. 3e). Higher values of $\frac{\gamma_{yield}}{\gamma_h}$ for pN1 microgels indicate that, at all the investigated ϕ, softer particles can accommodate more (relative) deformation before yielding. This effect is even more pronounced when looking at high deformation values corresponding to complete fluidization, which show a significant broadening of the yielding transition.

We can conclude that samples made of softer microgels start to deform and rearrange at lower strain values as a consequence of the lower sample elasticity (lower G', G'' values, associated with lower bulk moduli of the individual particles), however they can accommodate more (absolute) deformation before complete fluidization, presumably due to an increased ability of the particles to deform and interpenetrate to resist the applied deformation. Finally, for pN1 microgels, we also observe a decrease in the strain ratios (Fig. 3d, 3e) at higher ϕ. However, this decrease is shifted to higher volume fractions with respect to pN5. Softer microgels can reach higher effective volume fractions before the extent of single-particle deformation is so high that the microgels' ability to change their shape in response to the applied strain decreases and the deformation range between the onset of the yielding transition and complete fluidization progressively decreases.

3.3. Influence of the polymeric shell

We then investigated the influence of surface forces on the rheological behavior of microgels in dense states by adding linear PEG chains on their surface, while keeping the crosslinker content unchanged. We first note that the viscoelastic moduli of pN-PEG5 particles do not increase linearly with ϕ throughout the investigated regime (Fig. 4a). A similar result was obtained on copolymer pNIPAM-PEG microgels [36], and attributed to a saturation of interpenetration and shell compression at the highest ϕ, resulting in a more pronounced increase of G', although the relatively low number of points here precludes a more detailed analysis of the rheological behavior at small deformations. When comparing with pure pNIPAM microgels, the moduli are always lower in the presence of PEG for all ϕ investigated, albeit this difference decreases at the highest ϕ.

Based on the DLS results and the comparable de-swelling curves of the two microgels, we hypothesize that changes in the rheological behavior are mostly dependent on interparticle interactions in crowded environments and not on single-particle softness, which remains similar for the same crosslinker content. In particular, PEG chains on the microgels' surface, being more hydrophilic than pNIPAM, might decrease adhesion and friction between particles, similarly to what observed in the case of pNIPMAM (poly(N-isopropyl-methacrylamide)) and pNIPAM colloids [34]. This effect is particularly relevant at lower ϕ, when the microgels are less compressed and thus surface properties and interparticle contacts are expected to be more important in governing the rheological behavior, and it might explain the observed decrease of G' and G'' for pN-PEG5 with respect to the homopolymer particles.

The influence of PEG-mediated surface interactions is also affecting the non-linear response of the samples under LAOS (Fig. 4b-e, Figs. S9-S10). Differences between pN5 and pN-PEG5 microgels stand out especially when looking at the ratios $\frac{\gamma_{yield}}{\gamma_h}$ (Fig. 4d) and $\frac{\gamma_{fluid}}{\gamma_{yield}}$ (Fig. 4e). Up to $\phi < 1.2$, when the interactions between surfaces in contact dominate, the lower adhesion and friction between particles as mediated by the PEG chains results in samples that overall yield (Fig. 4d) and finally flow (Fig. 4e) in a lower deformation range. Instead, for $\phi > 1.2$,

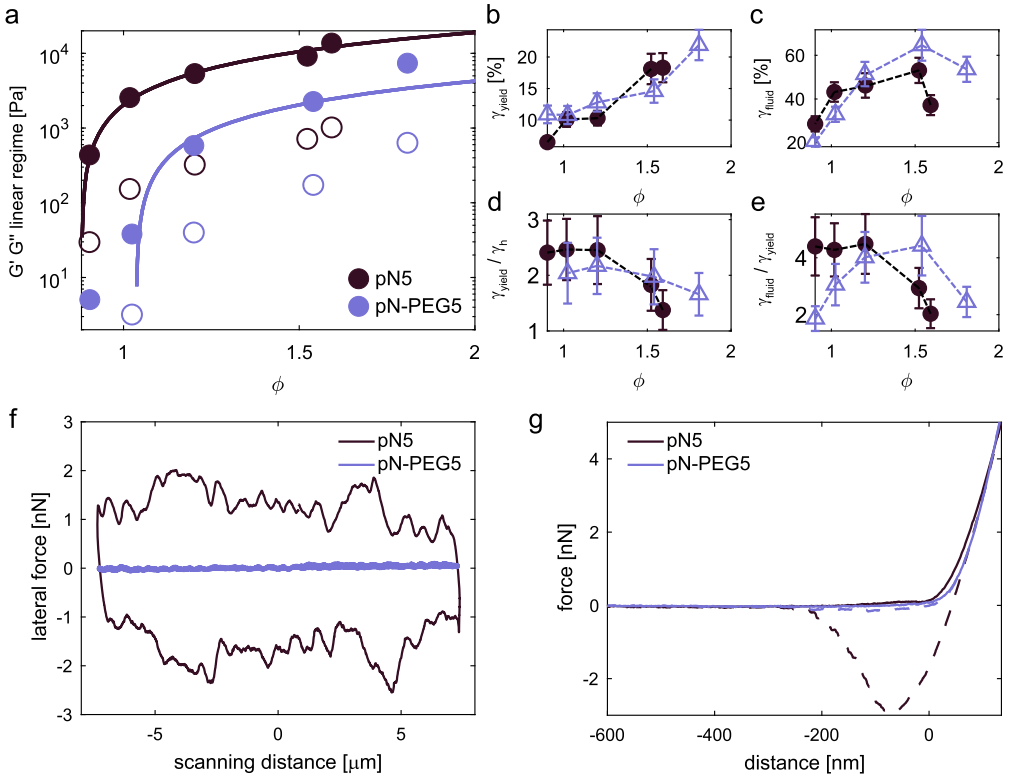

Fig. 4. Influence of the polymeric shell. a) Storage (filled symbols) and viscous (open symbols) moduli in the linear regime ($\gamma = 0.5 - 1\%$) as a function of ϕ (temperature = 25 °C, $\omega = 10$ rad/s). Solid lines represent linear fitting of the data. b) First strain value at which $\delta_t = \pi/4$ as a function of volume fraction. c) First strain value at which $\delta_t = \pi/2$ as a function of volume fraction. d) Strain ratio $\frac{\gamma_{yield}}{\gamma_h}$ as a function of volume fraction. e) Strain ratio $\frac{\gamma_{fluid}}{\gamma_{yield}}$ as a function of volume fraction. In b-e) pN5 filled circles, pN-PEG5 open triangles, dashed lines to guide the eye. f) Lateral force versus scanning distance (friction loops) for pN5 (black) and pN-PEG5 (violet) microgel monolayers deposited on a silicon wafer and immersed in water, obtained using colloidal probe atomic force microscopy (CP-AFM) at 25 °C under a normal load of 10 nN. See Materials and Methods for details. g) AFM force-vs-distance curves (approach curves solid lines, retraction curves dashed lines) obtained on the same microgel monolayers.

when the single-particle compression becomes more significant, the results resemble those obtained with pN1 microgels. However, while for pN1 microgels (Fig. 3) the different yielding behavior was attributed to the lower crosslinker content, in this case, we ascribe the more extended yielding process to the fuzziness, and thus resulting higher compliance, of the particle shell. Higher shell compliance enhances the microgels' ability to accommodate imposed deformations by rearranging with their neighbors, and, as a consequence, the yielding process is shifted to higher deformations.

In order to rationalize these observations, we turned to colloidal probe atomic force microscopy (CP-AFM) to characterize the friction and adhesion properties of microgel monolayers with and without PEG. To this end, we used lateral force microscopy and force measurements on monolayers of pN5 and pN-PEG5 microgels deposited on a silicon support and immersed in water at 25 °C. These measurements allow gaining information on the interfacial friction between the microgels' surface and the colloidal probe (silica colloid, diameter: 16 μm), as well as on the adhesion between the probe and the microgels [67]. In Fig. 4f we report friction loops (lateral force vs sliding distance) recorded by scanning the probe laterally over the microgel monolayers at a constant normal load of 10 nN. A comparable crosslinker content between the two samples rules out effects due to variations in the stiffness of the polymer layer, which in turn would affect the measured friction [67]. These data show that a very low friction is obtained in the case of monolayers of pN-PEG5, while pN5 microgels display a much higher friction, as visualized by the larger width of the friction loops. These observations are in agreement with previous studies indicating that PEG-coated surfaces tend to exhibit superior lubrication when compared to PNIPAM-coated surfaces in water at room temperature for the same grafting density, as measured by AFM [68–70].

In a complementary set of experiments, we used the same samples and tip to perform adhesion tests by indenting the microgel monolayers and recording the resulting force versus distance curves. As reported in Fig. 4g, we observe an appreciable adhesion between the tip and the surface of pN5 microgels, while pN-PEG5 microgels display very low adhesion. In the case of pNIPAM surfaces, the interaction upon contact with the silica colloid and subsequent compression is attributed to dehydration and polymer chains stretching during the probe retraction causing adhesion [71]. In contrast, lubricious PEG surface chains act as a barrier and prevent stretching of the chains reducing the adhesion with the probe. We note that the observed adhesion might have also contributed to the higher friction observed for the pN5 sample. Overall, these results indicate that both adhesion and friction are significantly decreased for pN-PEG microgels, strongly supporting the assumption that PEG chains are mainly located on the particle surface, and corroborating the interpretation of the rheological behavior.

Similar results have been obtained for microgels with 1 mol% crosslinker with and without PEG (Fig. S11). Also in this case, the friction for microgels containing PEG chains is lower and the adhesion is significantly decreased, indicating that PEG chains are covering the particle surface in contact with the colloidal probe, modifying the microgels' surface properties. We note that the increased friction between 5 mol% and 1 mol% samples can be attributed to the decreased stiffness of the microgel layer, and consequent higher deformation and resulting tip-sample contact area during compression with the colloidal probe [67]. Regarding the rheological properties of pN1 and pN-PEG1 microgels (Fig. S12), the results are overall coherent with what observed in the presence of a higher crosslinker content. The addition of PEG surface chains decreases even further the G' and G'' values in the linear regime, indicating that such particles behave as "ultra-soft" col-

loids in these experiments. Such an effect is particularly relevant in the lower concentration range investigated ($\phi < 1.2$), when the influence of surface contacts is emphasized. Although the response in the non-linear regime is too noisy for an accurate analysis due to the very low G' values obtained for pN-PEG1, also the trend at large deformations follows what observed when comparing stiffer particles with or without PEG surface chains (Fig. 4).

4. Conclusions

In this work, we investigated the rheological behavior of pNIPAM microgels under oscillatory shear, exploiting the sequence of physical processes [48,49] approach to the analysis of LAOS data to gain insight on the dynamics of the yielding transition spanning a broad range of applied strain amplitudes. Overall, these results provide additional insight on the complex viscoelastic properties of dense microgel suspensions, linking both particle elasticity (mediated by the crosslinker content) and interparticle contacts (dictated by the polymer chains on the particle surface) to the onset of yielding and to the overall transition from solid-like to fluid-like behavior.

While the linear viscoelastic moduli of dense microgel suspensions decrease upon lowering the bulk modulus of individual particles [29,33], we observe that particle softness plays an opposite role in the non-linear response. The deformation range required from the onset of the yielding transition up to complete sample fluidization increases for softer microgels. This is attributed to the fact that softer particles can accommodate more deformation before the sample yields and ultimately fluidifies. The incorporation of PEG chains on the particle surface can be used as an orthogonal way to lower the linear storage and loss moduli of the dense suspensions. This is attributed to a decrease in the adhesion and friction between particles when the surface-to-surface interactions are mediated by polymer chains that are more hydrophilic with respect to pNIPAM, as measured by using colloidal probe lateral force microscopy and force measurements on microgel monolayers deposited on a solid support. We note that a similar effect was reported when comparing pNIPAM and pNIPMAM microgels [34]. When subjected to shear deformation, the lubrication provided by the PEG chains induces a faster yielding transition. Finally, for all the investigated particles we observed that the samples at the highest packing fractions resist yielding up to higher deformations, but then fluidization is completed in a shorter deformation range. This indicates that, above a certain compression and deformation induced by crowding, the microgels decrease their ability to deform further when sheared, therefore resisting less to the imposed strain. Such behavior is shifted to higher packing fractions both for loosely crosslinked particles and for pNIPAM-PEG microgels due to their increased softness and fuzziness, respectively. Future works will be devoted to discern contributions to the overall interparticle interactions due to the pNIPAM core or the PEG shell at the microstructural level, where super-resolution microscopy or neutron scattering experiments can provide additional insight to the rheological investigation.

Overall, we believe these results can be of great potential value in discerning contributions due to particle elasticity and interparticle contacts that govern the viscoelastic properties of dense suspensions of soft particles subjected to shear. Providing novel tools to tune the mechanical and rheological behavior of such complex suspensions is of relevance for a large range of materials, processes and formulations containing soft colloids, either as main components or as additives, in order to modulate their functional properties [2,4]. Importantly, these results might have implications not only in understanding the behavior of polymeric microgels, but also in tuning other soft systems that are governed by a delicate interplay of surface contacts and particle compression, such as biodegradable soft colloids [72], self-assembled block copolymers [39] or star-polymers [73,74].

CRediT authorship contribution statement

Jacopo Vialetto: Writing – review & editing, Writing – original draft, Visualization, Validation, Resources, Project administration, Investigation, Funding acquisition, Formal analysis, Data curation, Conceptualization. **Shivaprakash N. Ramakrishna:** Writing – review & editing, Writing – original draft, Validation, Methodology, Investigation. **Lucio Isa:** Writing – review & editing, Resources, Funding acquisition, Conceptualization. **Marco Laurati:** Writing – review & editing, Writing – original draft, Supervision, Resources, Project administration, Methodology, Funding acquisition, Conceptualization.

Declaration of competing interest

The authors declare that they have no known competing financial interests or personal relationships that could have appeared to influence the work reported in this paper.

Data availability

Data will be made available on request.

Acknowledgements

The authors would like to thank S. Rogers for providing the codes for the SPP analysis. J.V. acknowledges funding from the European Union's Horizon 2020 research and innovation programme under the Marie Skłodowska Curie grant agreement 888076, ACRI (associazione di fondazioni e di casse di risparmio Spa) and Ministero dell'Università e della Ricerca (DM 247, grant MSCA_0000004), funded by European Union - NextGenerationEU - PNRR, Missione, 4 Componente, 2 Investimento 1.2.

Appendix A. Supplementary material

Supplementary material related to this article can be found online at https://doi.org/10.1016/j.jcis.2024.05.214.

References

[1] F. Scheffold, Pathways and challenges towards a complete characterization of microgels, Nat. Commun. 11 (2020) 4315.
[2] C. Ness, R. Seto, R. Mari, The physics of dense suspensions, Annu. Rev. Condens. Matter Phys. 13 (2022) 97–117.
[3] D. Vlassopoulos, M. Cloitre, Tunable rheology of dense soft deformable colloids, Curr. Opin. Colloid Interface Sci. 19 (2014) 561–574.
[4] A. Scotti, M.F. Schulte, C.G. Lopez, J.J. Crassous, S. Bochenek, W. Richtering, How softness matters in soft nanogels and nanogel assemblies, Chem. Rev. 122 (2022) 11675–11700.
[5] L. Li, J. Eyckmans, C.S. Chen, Designer biomaterials for mechanobiology, Nat. Mater. 16 (2017) 1164–1168.
[6] M. Hernando-Pérez, C. Zeng, M.C. Miguel, B. Dragnea, Intermittency of deformation and the elastic limit of an icosahedral virus under compression, ACS Nano 13 (2019) 7842–7849.
[7] Z. Hu, G. Huang, A new route to crystalline hydrogels, guided by a phase diagram, Angew. Chem., Int. Ed. 42 (2003) 4799–4802.
[8] T. Bhattacharjee, S.M. Zehnder, K.G. Rowe, S. Jain, R.M. Nixon, W.G. Sawyer, T.E. Angelini, Writing in the granular gel medium, Sci. Adv. 1 (2015) 4–10.
[9] A.M. Douglas, A.A. Fragkopoulos, M.K. Gaines, L.A. Lyon, A. Fernandez-Nieves, T.H. Barker, Dynamic assembly of ultrasoft colloidal networks enables cell invasion within restrictive fibrillar polymers, Proc. Natl. Acad. Sci. 114 (2017) 885–890.
[10] M. Najafi, M. Habibi, R. Fokkink, W.E. Hennink, T. Vermonden, LCST polymers with UCST behavior, Soft Matter 17 (2021) 2132–2141.
[11] M.A. da Silva, P. Haddow, S.B. Kirton, W.J. McAuley, L. Porcar, C.A. Dreiss, M.T. Cook, Thermoresponsive triblock-copolymers of polyethylene oxide and polymethacrylates: linking chemistry, nanoscale morphology, and rheological properties, Adv. Funct. Mater. 32 (2022).

[12] C.E. Miksch, N.P. Skillin, B.E. Kirkpatrick, G.K. Hach, V.V. Rao, T.J. White, K.S. Anseth, 4D printing of extrudable and degradable Poly(Ethylene Glycol) microgel scaffolds for multidimensional cell culture, Small 18 (2022).
[13] S. Jung, F. Meyer, S. Hörnig, M. Bund, B. Häßel, L.P.B. Guerzoni, L.D. Laporte, G.B. Messaoud, S.P. Centeno, A. Pich, On-Chip fabrication of colloidal suprastructures by assembly and supramolecular interlinking of microgels, Small 20 (2024).
[14] G.M. Conley, P. Aebischer, S. Nöjd, P. Schurtenberger, F. Scheffold, Jamming and overpacking fuzzy microgels: deformation, interpenetration, and compression, Sci. Adv. 3 (2017) e1700969.
[15] G.M. Conley, C. Zhang, P. Aebischer, J.L. Harden, F. Scheffold, Relationship between rheology and structure of interpenetrating, deforming and compressing microgels, Nat. Commun. 10 (2019) 2436.
[16] K. van der Vaart, Y. Rahmani, R. Zargar, Z. Hu, D. Bonn, P. Schall, Rheology of concentrated soft and hard-sphere suspensions, J. Rheol. 57 (2013) 1195–1209.
[17] B. Zhou, U. Gasser, A. Fernandez-Nieves, Poly(N-isopropylacrylamide) microgel swelling behavior and suspension structure studied with small-angle neutron scattering, Phys. Rev. E 108 (2023) 054604.
[18] V. Carrier, G. Petekidis, Nonlinear rheology of colloidal glasses of soft thermosensitive microgel particles, J. Rheol. 53 (2009) 245–273.
[19] D. Paloli, P.S. Mohanty, J.J. Crassous, E. Zaccarelli, P. Schurtenberger, Fluid–solid transitions in soft-repulsive colloids, Soft Matter 9 (2013) 3000.
[20] C. Pellet, M. Cloitre, The glass and jamming transitions of soft polyelectrolyte microgel suspensions, Soft Matter 12 (2016) 3710–3720.
[21] M.J. Bergman, N. Gnan, M. Obiols-Rabasa, J.-m.M. Meijer, L. Rovigatti, E. Zaccarelli, P. Schurtenberger, A new look at effective interactions between microgel particles, Nat. Commun. 9 (2018) 5039.
[22] A. Scotti, J.E. Houston, M. Brugnoni, M.M. Schmidt, M.F. Schulte, S. Bochenek, R. Schweins, A. Feoktystov, A. Radulescu, W. Richtering, Phase behavior of ultrasoft spheres show stable bcc lattices, Phys. Rev. E 102 (2020) 052602.
[23] S.V. Nikolov, A. Fernandez-Nieves, A. Alexeev, Behavior and mechanics of dense microgel suspensions, Proc. Natl. Acad. Sci. 117 (2020) 27096–27103.
[24] A. Scotti, S. Bochenek, M. Brugnoni, M.A. Fernandez-Rodriguez, M.F. Schulte, J.E. Houston, A.P.H. Gelissen, I.I. Potemkin, L. Isa, W. Richtering, Exploring the colloid-to-polymer transition for ultra-low crosslinked microgels from three to two dimensions, Nat. Commun. 10 (2019) 1418.
[25] J. Vialetto, F. Camerin, F. Grillo, S.N. Ramakrishna, L. Rovigatti, E. Zaccarelli, L. Isa, Effect of internal architecture on the assembly of soft particles at fluid interfaces, ACS Nano 15 (2021) 13105–13117.
[26] J. Vialetto, N. Nussbaum, J. Bergfreund, P. Fischer, L. Isa, Influence of the interfacial tension on the microstructural and mechanical properties of microgels at fluid interfaces, J. Colloid Interface Sci. 608 (2022) 2584–2592.
[27] A.S.J. Iyer, L.A. Lyon, Self-healing colloidal crystals, Angew. Chem., Int. Ed. 48 (2009) 4562–4566.
[28] A. Scotti, U. Gasser, E.S. Herman, J. Han, A. Menzel, L.A. Lyon, A. Fernandez-Nieves, Phase behavior of binary and polydisperse suspensions of compressible microgels controlled by selective particle deswelling, Phys. Rev. E 96 (2017) 032609.
[29] A. Scotti, M. Brugnoni, C.G. Lopez, S. Bochenek, J.J. Crassous, W. Richtering, Flow properties reveal the particle-to-polymer transition of ultra-low crosslinked microgels, Soft Matter 16 (2020) 668–678.
[30] M.V. Saisavadas, S. Dhara, R.G. Joshi, B.V.R. Tata, Large amplitude oscillatory shear studies on dense PNIPAM microgel colloidal glasses, Colloid Polym. Sci. 301 (2023) 599–611.
[31] G. Romeo, A. Fernandez-Nieves, H.M. Wyss, D. Acierno, D.A. Weitz, Temperature-controlled transitions between glass, liquid, and gel states in dense p-NIPA suspensions, Adv. Mater. 22 (2010) 3441–3445.
[32] G. Chaudhary, A. Ghosh, J.G. Kang, P.V. Braun, R.H. Ewoldt, K.S. Schweizer, Linear and nonlinear viscoelasticity of concentrated thermoresponsive microgel suspensions, J. Colloid Interface Sci. 601 (2021) 886–898.
[33] P. Menut, S. Seiffert, J. Sprakel, D.A. Weitz, Does size matter? Elasticity of compressed suspensions of colloidal- and granular-scale microgels, Soft Matter 8 (2012) 156–164.
[34] K. Urayama, T. Saeki, S. Cong, S. Uratani, T. Takigawa, M. Murai, D. Suzuki, A simple feature of yielding behavior of highly dense suspensions of soft micro-hydrogel particles, Soft Matter 10 (2014) 9486–9495.
[35] J.A. Moreno-Guerra, I.C. Romero-Sánchez, A. Martinez-Borquez, M. Tassieri, E. Stiakakis, M. Laurati, Model-free rheo-AFM probes the viscoelasticity of tunable DNA soft colloids, Small 15 (2019).
[36] M. Lara-Peña, A. Licea-Claverie, I. Zapata-González, M. Laurati, Colloidal and polymeric contributions to the yielding of dense microgel suspensions, J. Colloid Interface Sci. 587 (2021) 437–445.
[37] A. Guerron, S. Giasson, Multiresponsive microgels: toward an independent tuning of swelling and surface properties, Langmuir 37 (2021) 11212–11221.
[38] J. Ruiz-Franco, R. Rivas-Barbosa, M.A. Lara-Peña, J.R. Villanueva-Valencia, A. Licea-Claverie, E. Zaccarelli, M. Laurati, Concentration and temperature dependent interactions and state diagram of dispersions of copolymer microgels, Soft Matter 19 (2023) 3614–3628.
[39] M.T. Cook, P. Haddow, S.B. Kirton, W.J. McAuley, Polymers exhibiting lower critical solution temperatures as a route to thermoreversible gelators for healthcare, Adv. Funct. Mater. 31 (2021).
[40] A. Prause, M. Hechenbichler, R.F. Schmidt, M. Simon, S. Prévost, L.P. Cavalcanti, Y. Talmon, A. Laschewsky, M. Gradzielski, Rheological control of aqueous dispersions by thermoresponsive BAB* copolymers of different architectures, Macromolecules 56 (2023) 104–121.
[41] J. Clara-Rahola, A. Fernandez-Nieves, B. Sierra-Martin, A.B. South, L.A. Lyon, J. Kohlbrecher, A.F. Barbero, Structural properties of thermoresponsive poly(N-isopropylacrylamide)-poly(ethyleneglycol) microgels, J. Chem. Phys. 136 (2012) 214903.
[42] V.F. Motlaq, K.D. Knudsen, B. Nyström, Effect of PEGylation on the stability of thermoresponsive nanogels, J. Colloid Interface Sci. 524 (2018) 245–255.
[43] C.L.A. Berli, D. Quemada, Rheological modeling of microgel suspensions involving solid-liquid transition, Langmuir 16 (2000) 7968–7974.
[44] D. Li, R. Hsu, B. Figura, R. Jacobs, S. Li, S. Horvath, T. Clifford, K. Chari, Rheology and structure of surface crosslinked surfactant-activated microgels, Soft Matter 12 (2016) 7150–7158.
[45] K. Hyun, M. Wilhelm, C.O. Klein, K.S. Cho, J.G. Nam, K.H. Ahn, S.J. Lee, R.H. Ewoldt, G.H. McKinley, A review of nonlinear oscillatory shear tests: analysis and application of large amplitude oscillatory shear (LAOS), Prog. Polym. Sci. 36 (2011) 1697–1753.
[46] N. Koumakis, A. Pamvouxoglou, A.S. Poulos, G. Petekidis, Direct comparison of the rheology of model hard and soft particle glasses, Soft Matter 8 (2012) 4271–4284.
[47] R.G. Joshi, B.V.R. Tata, Sub-diffusive dynamics and two-step yielding in dense thermo-responsive microgel glasses, Colloid Polym. Sci. 295 (2017) 1671–1683.
[48] S.A. Rogers, In search of physical meaning: defining transient parameters for nonlinear viscoelasticity, Rheol. Acta 56 (2017) 501–525.
[49] G.J. Donley, J.R. de Bruyn, G.H. McKinley, S.A. Rogers, Time-resolved dynamics of the yielding transition in soft materials, J. Non-Newton. Fluid Mech. 264 (2019) 117–134.
[50] J. Vialetto, S.N. Ramakrishna, L. Isa, In situ imaging of the three-dimensional shape of soft responsive particles at fluid interfaces by atomic force microscopy, Sci. Adv. 8 (2022) eabq2019.
[51] J.L. Hutter, J. Bechhoefer, Calibration of atomic-force microscope tips, Rev. Sci. Instrum. 64 (1993) 1868–1873.
[52] C.P. Green, H. Lioe, J.P. Cleveland, R. Proksch, P. Mulvaney, J.E. Sader, Normal and torsional spring constants of atomic force microscope cantilevers, Rev. Sci. Instrum. 75 (2004) 1988–1996.
[53] R.J. Cannara, M. Eglin, R.W. Carpick, Lateral force calibration in atomic force microscopy: a new lateral force calibration method and general guidelines for optimization, Rev. Sci. Instrum. 77 (2006).
[54] N.A. Bharadwaj, R.H. Ewoldt, Single-point parallel disk correction for asymptotically nonlinear oscillatory shear, Rheol. Acta 54 (2015) 223–233.
[55] A.J. Giacomin, P.H. Gilbert, D. Merger, M. Wilhelm, Large-amplitude oscillatory shear: comparing parallel-disk with cone-plate flow, Rheol. Acta 54 (2015) 263–285.
[56] H.Y. Song, R. Salehiyan, X. Li, S.H. Lee, K. Hyun, A comparative study of the effects of cone-plate and parallel-plate geometries on rheological properties under oscillatory shear flow, Korea-Aust. Rheol. J. 29 (2017) 281–294.
[57] J. Es Sayed, C. Lorthioir, P. Perrin, N. Sanson, PEGylated NiPAM microgels: synthesis, characterization and colloidal stability, Soft Matter 15 (2019) 963–972.
[58] P. Agnihotri, R. Raj, D. Kumar, A. Dan, Short oligo(ethylene glycol) chain incorporated thermoresponsive microgels: from structural analysis to modulation of solution properties, Soft Matter 16 (2020) 7845–7859.
[59] F. Scheffold, P. Díaz-Leyva, M. Reufer, N. Ben Braham, I. Lynch, J.L. Harden, Brush-like interactions between thermoresponsive microgel particles, Phys. Rev. Lett. 104 (2010) 128304.
[60] G. Romeo, M.P. Ciamarra, Elasticity of compressed microgel suspensions, Soft Matter 9 (2013) 5401–5406.
[61] A. Zaccone, E. Scossa-Romano, Approximate analytical description of the nonaffine response of amorphous solids, Phys. Rev. B 83 (2011) 184205.
[62] G.J. Donley, P.K. Singh, A. Shetty, S.A. Rogers, Elucidating the G" overshoot in soft materials with a yield transition via a time-resolved experimental strain decomposition, Proc. Natl. Acad. Sci. 117 (2020) 21945–21952.
[63] J.M. Brader, M. Siebenbürger, M. Ballauff, K. Reinheimer, M. Wilhelm, S.J. Frey, F. Weysser, M. Fuchs, Nonlinear response of dense colloidal suspensions under oscillatory shear: mode-coupling theory and Fourier transform rheology experiments, Phys. Rev. E 82 (2010) 061401.
[64] D. Bonn, M.M. Denn, L. Berthier, T. Divoux, S. Manneville, Yield stress materials in soft condensed matter, Rev. Mod. Phys. 89 (2017) 035005.
[65] A. Ghosh, G. Chaudhary, J.G. Kang, P.V. Braun, R.H. Ewoldt, K.S. Schweizer, Linear and nonlinear rheology and structural relaxation in dense glassy and jammed soft repulsive pNIPAM microgel suspensions, Soft Matter 15 (2019) 1038–1052.
[66] K. Kaithakkal Jathavedan, F. Kanheerampockil, S. Bhat, Role of particle morphology in the yielding behavior of dense thermosensitive microgel suspensions, J. Appl. Polym. Sci. 137 (2020) 48625.
[67] E. Liamas, S.D. Connell, S.N. Ramakrishna, A. Sarkar, Probing the frictional properties of soft materials at the nanoscale, Nanoscale 12 (2020) 2292–2308.
[68] M.A. Brady, F.T. Limpoco, S.S. Perry, Solvent-dependent friction force response of Poly(ethylenimine)- graft -poly(ethylene glycol) brushes investigated by atomic force microscopy, Langmuir 25 (2009) 7443–7449.
[69] S.N. Ramakrishna, R.M. Espinosa-Marzal, V.V. Naik, P.C. Nalam, N.D. Spencer, Adhesion and friction properties of polymer brushes on rough surfaces: a gradient approach, Langmuir 29 (2013) 15251–15259.

[70] G. Morgese, Y. Gombert, S.N. Ramakrishna, E.M. Benetti, Mixing Poly(ethylene glycol) and Poly(2-alkyl-2-oxazoline)s enhances hydration and viscoelasticity of polymer brushes and determines their nanotribological and antifouling properties, ACS Appl. Mater. Interfaces 10 (2018) 41839–41848.
[71] G. Li, I. Varga, A. Kardos, I. Dobryden, P.M. Claesson, Nanoscale mechanical properties of core–shell-like Poly-NIPAm microgel particles: effect of temperature and cross-linking density, J. Phys. Chem. B 125 (2021) 9860–9869.
[72] V. Rathee, J. Miller, D.L. Blair, J.S. Urbach, Structure of propagating high-stress fronts in a shear-thickening suspension, Proc. Natl. Acad. Sci. 119 (2022).
[73] J. Zhang, P.M. Lettinga, J.K. Dhont, E. Stiakakis, Direct visualization of conformation and dense packing of DNA-based soft colloids, Phys. Rev. Lett. 113 (2014) 268303.
[74] I. Romero-Sanchez, I. Pihlajamaa, N. Adžić, L.E. Castellano, E. Stiakakis, C.N. Likos, M. Laurati, Blunt-End driven re-entrant ordering in quasi two-dimensional dispersions of spherical DNA brushes, ACS Nano 16 (2022) 2133–2146.